Heliyon 9 (2023) e18925

Contents lists available at ScienceDirect

Heliyon

journal homepage: www.cell.com/heliyon

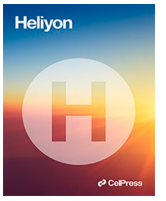

Preparation and characterization of indoor heat blockage panel composites made of polyurethane-hybrid-foam-concrete and rice-husk-ash

Jofrishal Jofrishal [a,b], Muhammad Adlim [a,c,*], Elin Yusibani [d], Akhyar Akhyar [e], Ratu Fazlia Inda Rahmayani [c], Rahmatul Fajri [f]

[a] Graduate School of Mathematics and Applied Science, Universitas Syiah Kuala, Banda Aceh, 23111, Indonesia
[b] Chemistry Department, Faculty of Teacher Training and Education, Universitas Samudra, Langsa, 24415, Indonesia
[c] Chemistry Department, Faculty of Teacher Training and Education, Universitas Syiah Kuala, Banda Aceh, 23111, Indonesia
[d] Physics Department, Faculty of Mathematics and Natural Sciences, Universitas Syiah Kuala, Banda Aceh, 23111, Indonesia
[e] Mechanical Engineering Department, Faculty of Engineering, Universitas Syiah Kuala, Banda Aceh, 23111, Indonesia
[f] Chemistry Department, Faculty of Engineering, Universitas Samudra, Langsa, 24415, Indonesia

ARTICLE INFO

Keywords:
Solar heat blockage
Indoor wall panel
Hybrid-foam-concrete
White portland cement
Rice-husk-ash
Mechanical properties

ABSTRACT

The preferable properties of indoor heat blockage material for tropical environments are blocking outside heat without absorbing and storing it inside the blockage material, therefore studying the component and the composite properties are crucial. This study, therefore, aims to prepare and characterize a new hybrid foam concrete based on Rice Husk Ash (RHA) composite panels as an indoor building material called Hybrid Foam Panel (HFP). Polyurethane made of the combination of blended polyol (catalyst and surfactant) and diphenylmethane-4,4′-diisocyanate with a constant proportion was used as a matrix, while white Portland cement and RHA with various compositions were used as fillers. The formation of polyurethane foam and related chemical reactions are confirmed and RHA in HFP composition gave significant roles in composite properties. HFP made with the right constituent composition caused much lower thermal conductivity (down to 0.22 W/mK) than the control, blocked the IR radiation heat, and it has moderate compressive strength. HFP with RHA content in consolidated parameters shows a compressive strength of 7.25–12.37 MPa; densities of 1216–1351 kg/m^3 and a porosity of 62%. HFP also stands for heat at least 300 °C, thereby it is a potential interior solar heat blockade, especially in the tropical region.

1. Introduction

The environmental temperature escalation in urban areas is one of the worldwide issues, especially in tropical regions that receive year-round sunlight. The increased watertight areas, domestic energy use, vegetation reduction, increased anthropogenic energy waste, use of inappropriate building construction materials, and roads/paving are all contributing factors to discomfort [1]. The use of conventional bricks not only contributes excessive heat to the environment [2] but also stores heat for a certain period, which will be released overnight when the ambient temperature turns colder [3]. Therefore, continuous air conditioning (AC) is required to cool

* Corresponding author. Graduate School of Mathematics and Applied Science, Universitas Syiah Kuala, Banda Aceh, 23111, Indonesia.
E-mail addresses: adlim@usk.ac.id, adlim@unsyiah.ac.id (M. Adlim).

https://doi.org/10.1016/j.heliyon.2023.e18925
Received 5 February 2023; Received in revised form 28 July 2023; Accepted 2 August 2023
Available online 3 August 2023

houses, which releases more heat into the environment. Sunlight has component radiations, including IR, Visible, and Ultraviolet (UV), but IR is the most significant proportion and the major contributor to heat elevation. The formula of solar heat-blockage materials has been intensively investigated to solve this problem, including hybridizing concrete, polymer, and rice husk ash (RHA). Hybridization aims to improve thermal insulation in concrete components, however, the component proportion will affect the concrete strength and durability [4]. Heat block materials are also prepared as phase change materials (PCMs) [5]. Low melting point matter absorbs heat and then uses the heat to change phase. The heat releases back when the matter returns to the initial phase. Therefore heat is stored to warm indoors at night, which is ideal property of heat-blockage material used in subtropical regions.

Unlike in subtropical climates, where hot weather occurs day and night, the preferable property of indoor heat blockage material for tropical environments is insulating the warm wall but minimalizing the heat absorption. Therefore studying the component and the composite properties are crucial.

Since thermal insulation properties depend on thermal transport via the gas phase within their pores [6], the pore structures of the building material are crucial to study. One of the materials that generate pores and low thermal conductivity is polyurethane. Polyurethane has good fluidity, is lightweight, and has low thermal conductivity [7,8], so it is often used as a base material mixed with Portland cement and is known as hybrid foam. This composite can be applied indoors or outdoors in the building. It is also an excellent heat sink, has good mechanical strength, and is resistant to acids, fires, and earthquakes [9–12]. The hybrid foam is usually spray coating, not wall panels, which can be assembled artistically. Also, the high proportion of polyurethane might decrease the composite strength.

Several studies on foam concrete involving rice husk ash (RHA) as the component have been available in recent literature [13,14]. Using RHA in the composite relates to high silica content (85–95%) in RHA. Also, RHA increased concrete durability, strength, and permeability [15–17] and reduced thermal conductivity [18,19]. Also, the pozzolanic activity of RHA in concrete corresponds with the composite characteristic improvement [15].

RHA has been proven essential in brick and clay-roof-tile production, improving brick-and-mortar performance [19,20]. The presence of RHA in the brick matrix also reduced thermal and noise interference from the environment [21,22]. The RHA is also compatible with several materials, including palm kernel shells, concrete [23], epoxy resin, and Araldite [24].

When RHA was mixed with polyethylene glycol, the composite functioned as heat storage instead of heat blockage [25]. Based on the literature review a foam composite containing RHA, polyurethane, and white Portland cement as an indoor panel has not been much studied. The combination of these materials shall improve the individual component characteristics and generate a better performance of the composite. This solar-heat-blockage indoor panel easily assembled with existing house-wall, made of local materials, is well-being, and relatively environmentally friendly are promising.

Polyurethane, a hybrid foam in the composite matrix, is synthesized by the condensation reaction between isocyanate and polyol. The interaction between the isocyanate group, which contains active hydrogen, and the hydroxyl group of the polyol compound with several cross-linked urethane compounds results in the urethane monomer. Chemically, polyurethane is thermoplastic and thermoset, while physically, this compound has a rigid, porous structure and soft elastomer. These forms rely on the type or specifications of the isocyanate, polyol, and the percentage of mixture ratio [26].

Polyurethane uses as a matrix in cement has been reported previously [7], and the combination of cement filler and RHA (in the right proportion) enhanced the strength of concrete [27,28]. It is due to the silica content within RHA, which has reactivity and is known as a pozzolanic material. The silica increases mechanical strength and modifies the thermal properties of concrete [15,29]. Further, hybrid polyurethane foam mixed with red carbon mud as a filler made composite resistant to fire and has good thermal stability and electromagnetic interference shield [30].

On the other hand, white Portland cement contains more CaO compounds (66–67%) and fewer Fe_2O_3 (0.21–0.24%) [30] compared to the grey cement content. White cement also has low thermal conductivity (0.75 W/mK) [31]. Lowering thermal conductivity can save natural resources and energy and reduce carbon dioxide emissions [32]. Hence, studying the right composition and components in the composite synthesis will give desirable properties, such as low thermal conductivity, lightweight, strength, heat resistance, and others [15].

In this current study, RHA was mixed with polyurethane and white Portland cement (WPC) as indoor wall panels for heat insulation, which is in demand in tropical region buildings. This study explores the appropriate formula of RHA, polyurethane, and white Portland cement composite to optimize the thermal insulating properties and the mechanical and chemical characteristics.

2. Material and method

2.1. Material and instrument

The materials used in this research were blended polyol (mixture of glycerol and catalyst, bought from RigiChem-Singapore), Diphenylmethane-4,4′-diisocyanate (Merck-Germany), white Portland cement type I ASTM C 150-04a (Tiga Roda-Indonesia), and rice husk ash from rice mills in East Aceh (Aceh Province-Indonesia).

Several instruments were utilized in characterization, including analytical weight (Ohaus PA 224), oven (Memmert UN 30), mixer overhead stirrer (Chem equipment LKSC-B), sieve-100 mesh (CU Class A), Fourier-Transform Infrared Spectrometer (FTIR) (Thermo scientific Nicolet iS-10), Scanning Electron Microscope (SEM) (JEOL JSM-6510LA), X-ray Diffraction (XRD) (Shimadzu XD 610), X-Ray Fluorescence (XRF) (Panalytical Epsilon 3 XLE), Thermal Gravimetry Analysis (TGA) (PerkinElmer TGA 4000), digital thermometer (Hanna), Furnace (Thermo Scientific), and Compressive Testing Machine.

2.2. Preparation of the RHA

RHA samples were obtained from the waste of a local rice milling and processing factory in East Aceh Regency, Aceh Province, Indonesia (5°00′56.8″N 97°38′17.6″E). The rice husk waste was usually slowly burned in the open air (nearly without smog) but in uncontrolled combustion conditions, and it turned to black carbon, then became white ash. The combustion temperature is predicted by observing the color change of the RHA product after combustion. According to Jaya et al. [33] variations in combustion temperature produced different RHA colors. Grey-white color with a burning temperature of 500 °C and bright white at 800 °C. The RHA was taken randomly from several sides of the pile. It was cleaned for impurities before being grounded and sieved utilizing a 100-mesh sieve. XRD and XRF methods were utilized to characterize the main chemical compounds of RHA powder.

2.3. Preparation of the hybrid foam panel (HFP) and their characterization

HFP was generated with polyurethane (PU) which is the reaction product between a blended polyol and diphenylmethane-4,4-diisocyanate. Two-stage mixing approach was conducted in HFP preparation. In the first step, the cement was mixed with the polyol, stirring at 350 RPM for 15 min using an electrical lab mixer (overhead stirrer 50 Hz Chemical 200 w). The second step involved adding diphenylmethane-4,4-diisocyanate to the mixture and stirring it at 350 rpm for 15 min. The volume ratio between diphenylmethane-4,4-diisocyanate and polyol was set to 1:2. The weight ratio of PU (Polyol + Isocyanates) to (RHA + cement) in this work is set constant at 0.3, while the ratio of water-to-cement ratio is from 0.2 to 0.6 as has referred to the previous studies [34–36]. The variety in the amount of water is required according to the quantity of the solid components to maintain the homogeneity of the mixture. After that, all specimens were air-dried for 28 days of curing. In the specimen preparation, RHA was added as a filler in weight composition of 0, 5, 10, 15, 20, and 50% w/w from the total specimen weight. The HFP formula is set to refer to the literature [15,17,37], which is shown in Table 1, and the fresh paste was poured into a mold with a dimension of 150 × 25 × 10 mm. The samples were then put to the test for heat absorption. To prepare the samples for the mechanical properties to test using ASTM C-109-02, a mold of 50 × 50 × 50 mm was employed [38,39].

A circular shape sample (diameter = 60 cm; thickness = 5 cm) was prepared for thermal conductivity measurement using the hot disc method modified from ISO 22007–2 (calculations with equations (1) and (2)).

$$Q \approx A\frac{\Delta T}{\Delta x} \tag{1}$$

$$Q = \frac{dQ}{dt} = kA\frac{\Delta T}{\Delta x} \tag{2}$$

where Q is the heat flow rate (W = joule/s), ΔT is the temperature gradient (^{o}C), k is the thermal conductivity (W/mK), A is the cross-section area (m^2), and Δx is the thickness of the specimen (m) [40]. The HFP specimens were subjected to a thermal conduction test (Fig. 1a) within a closed cylindrical Styrofoam with dimensions of d = 60 cm and h = 20 cm. A hot plate equipped with a digital thermostat was used as the electrical heat source, and the temperature was maintained at 60 ± 2 °C. Afterward, the HFP specimen was inserted between two metal-equipped digital temperature measurement reference discs. Both reference discs utilized were the ASTM A 36 iron plates. The upper disc was then covered with a Styrofoam layer to avoid heat loss, as illustrated in Figure (1b). Overall, the thermal conductivity measurement schema is depicted in Fig. 1.

A thermal radiation test of the HFP specimen was conducted in a Styrofoam box with dimensions and experimental setup illustrated in Fig. 2. Thermal performance tests were also performed to determine the heat absorbed by the composite from IR radiation. Heat absorption was then measured by irradiating the sample with a 250-W IR lamp. For that, 180 min were spent irradiating (heating), followed by 130 min of cooling. Every 30 min, the data were recorded using a type k thermocouple connected to a data-hold-thermometer, as displayed in Fig. 2.

Meanwhile, to determine the density of HFP, the technique employed refers to ASTM C567-05a (2005) and SNI 3402 (2008) standards, and the porosity of HFP was carried out based on the ASTM C 642–06 (2008). The sample characterization involved several instrumentations such as FTIR, SEM, TGA, and XRD.

Table 1
Variation of rice husk ash as the filler and the hybrid foam characteristics.

Sample codes	RHA (%) in cement	RHA (g)	Cement (g)	Polyol (mL)	Isocyanates (mL)	Water (mL)
HFP 0	0	0.0	290	30	60	60
HFP 5	5	14.5	276	30	60	73
HFP 10	10	29.0	261	30	60	73
HFP 15	15	43.5	246	30	60	75
HFP 20	20	58.0	232	30	60	77
HFP 50	50	145.0	145	30	60	85
HFP 100	100	290.2	0	30	60	110

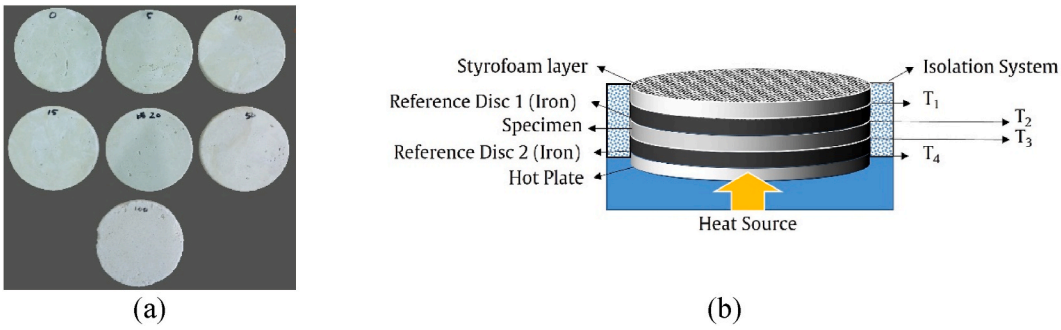

Fig. 1. (a) HFP Specimens and (b) Thermal conductivity measurement scheme.

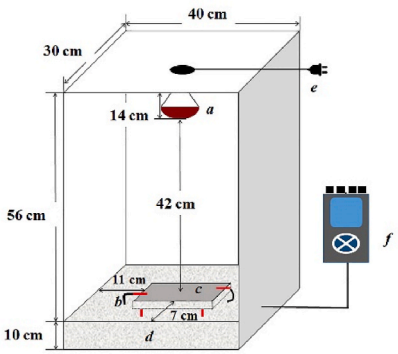

a = Infra-red lamp 250 watt
b = Type k Thermocouple
c = Hybrid panel
d = Styrofoam
e = Electrical connector
f = Thermometer data hold

Fig. 2. Infra-Red irradiation test scheme.

3. Result and discussion

Elaboration of the research finding started with the chemical composition of the composite component especially SiO_2 quantity and characteristics affecting the composite properties as summarized in Fig. 3.

Before elaborating on the HFP characteristic, RHA as the constituent component is discussed. The RHA is white material which is different from the raw rice husk as presented in Fig. 4 (b & c).

Fig. 4 (a) represents the RHA diffractogram showing the high crystallinity properties of the RHA component. The XRF data (Table 2) show RHA had high SiO_2 content (95%) compared to the other. Three types of silica compounds existed in the form of tridymite ($2\theta = 18.7°$, $20.7°$, $23.4°$, and $30.2°$), quartz ($2\theta = 21.8°$ and $27.6°$), and cristobalite ($2\theta = 31.6°$ and $36.2°$). The silica content in RHA from this study is consistent with earlier reports [20,21,32,41,42]. The silica content in RHA is higher than in meta-kaolin and analcime, which is naturally high silica content clay.

This high proportion and crystallinity of SiO_2 would have strengthened the durability, strength, and permeability as verified in the

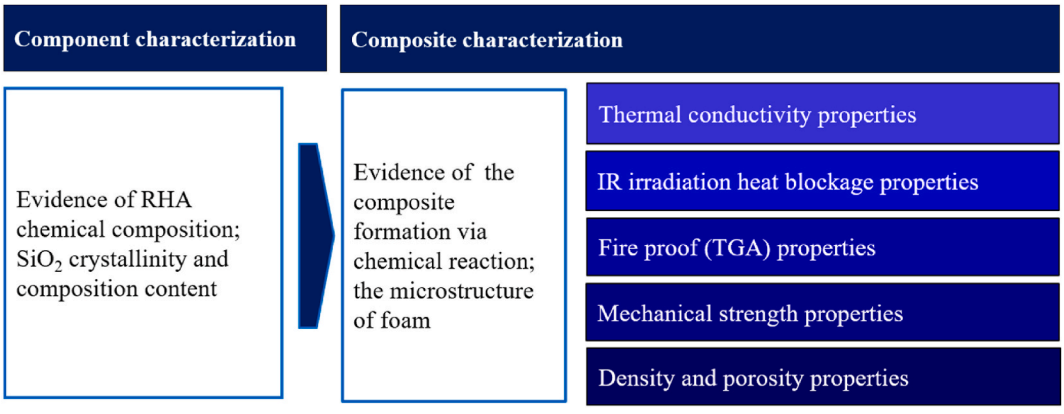

Fig. 3. The summary of HFP characterization methods and the parameter comparison.

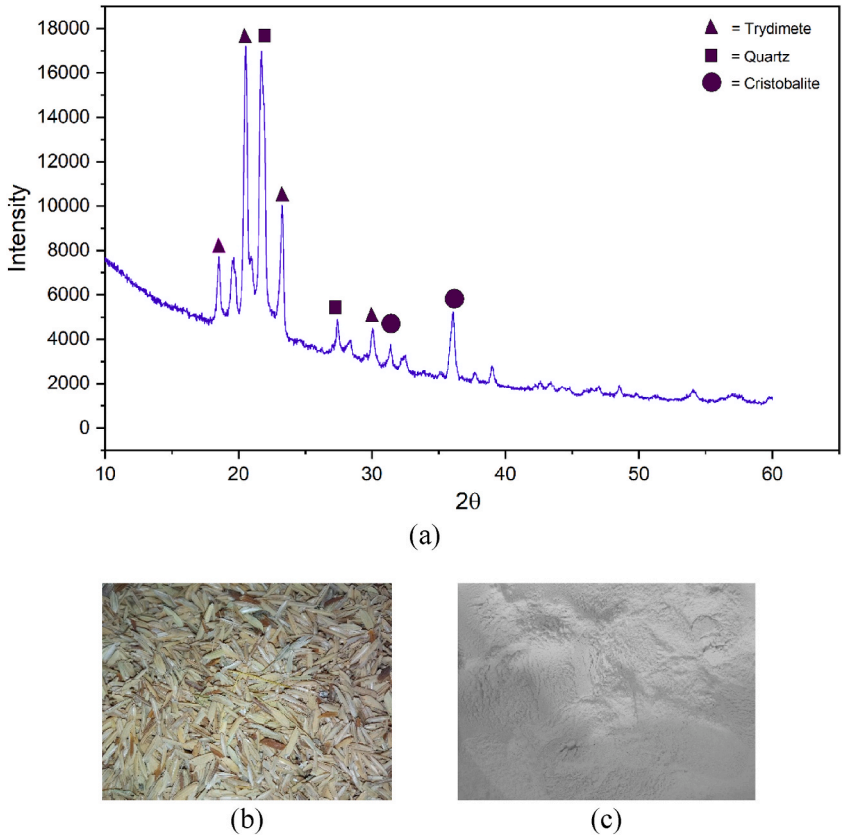

Fig. 4. (a) Diffractogram of RHA, (b) Rice husk raw material, (c) Rice husk ash after grinding and sifting.

Table 2
Composition of oxide compounds in RHA and WPC samples according to XRF method.

Compound	RHA		WPC	
	Concentration	Unit	Concentration	Unit
SiO_2	95.709	%	11.799	%
SO_3	–		2.526	%
P_2O_5	1.395	%	–	
Al_2O_3	–		2.623	%
K_2O	1.206	%	0.460	%
CaO	1.290	%	81.366	%
TiO_2	112.9	ppm	0.175	%
MnO	0.204	%	109.4	ppm
Fe_2O_3	0.132	%	0.592	%
Rb_2O	137.3	ppm	15.0	ppm
SrO	38.8	ppm	0.382	%

previous report [15–17]. The appropriate SiO_2 characteristic contributes to the thermal conductivity reduction of the HFP composite [18,21].

3.1. Microstructure analysis of hybrid foam panel (HFP) sample

In measuring the several parameters of treated samples, some assumptions are considered. The rate of chemical formation of polyurethane is assumpted constant at every replication, therefore the density of the composite is uniform. This possible experimental error has been minimized by several sample replications.

Fabricating a heat block material usually involves expanding the composite pores in the form of foam [43]. Polyurethane produces a foam from the precursor reaction between isocyanate and polyol. The size of foam bubbles might be affected by the presence of Portland cement and water content, therefore the chemical evidence and the composite surface properties are discussed here.

As presented in Table 1 and in the hybrid structure, the polyurethane was set constant (polyol and isocyanate; 30 and 60 mL), and

the Portland cement and RHA were given in various proportions with a total weight of 290 g. Then, about 60–70 mL of distilled water was added. It was found that the mixture immediately became hard after the reaction of polyol and isocyanate. Then, experiments were re-adjusted; HFP components were mixed homogeneously before the isocyanate addition.

Without RHA content, the polyurethane foam panel showed a granular structure. The thin layer fibers had not existed, and the foam was evenly distributed with a larger foam size and produced large pores. These granular shapes indicated hybrid foam characteristics. As seen in reaction 1, the foam was a reaction product of polyols, isocyanate, and water. When the isocyanate reacted with water (reaction 2), carbon dioxide gas was generated and trapped within the foam bubbles. The reaction mechanism is illustrated in Fig. 5.

Randomly, several HFP samples were carefully sliced using a grinding machine and left one site as the original surface. The original surface was cleaned before SEM scanning for microstructure studies at a 1000× and 5000× magnification scale. The SEM images (Fig. 6a–d) show the polyurethane foam containing RHA looks granules and spread (Fig. 6a and c) and such images were different from the SEM pictures of HFP without RHA content. The images also show a needle-shaped inorganic cement layer covering the granules within the samples. This finding is analogous to the microstructure of previous polyurethane-RHA samples prepared with different procedures previously [44,45]. The smaller grains and more porous fibrous observed in the HFP containing RHA aligned with the theory of SiO_2 role in strengthening the concrete structure [16,17]. Fibrous sheets are observed in Fig. 6 (a & c) confirming the formation of $CaSiO_3.3H_2O$ (calcium silicate hydrate/C–S–H). The reaction occurs after Portland cement chemical content is mixed with SiO_2 from RHA.

3.2. Fourier transform infrared spectroscopy (FTIR) analysis

Attempt to study the chemical reaction within HFP samples were carried out based on FTIR spectroscopic method. FTIR spectra record several chemical functional groups that are involved in reactions 1 and 2. The polyurethane formation is confirmed after spectra of the stretching of N–H, C═O, HNCOO, CH_2 bending, and C–*O*–C [46] are observed in The FTIR spectra (Fig. 7). It showed high intensity in 3400 cm^{-1} representing the N–H stretching; the C═O stretching appeared in 1700 cm^{-1}, CH_2 bending was in the area 2270 cm^{-1}, and urethane-specific groups (NHCOO) were found in 1509–1600 cm^{-1}. Several low-intensity peaks around 1413 cm^{-1} were identified as C–H bending and at 1600 cm^{-1} as C═N-. These data confirm the hypothesis that a reaction occurs to form

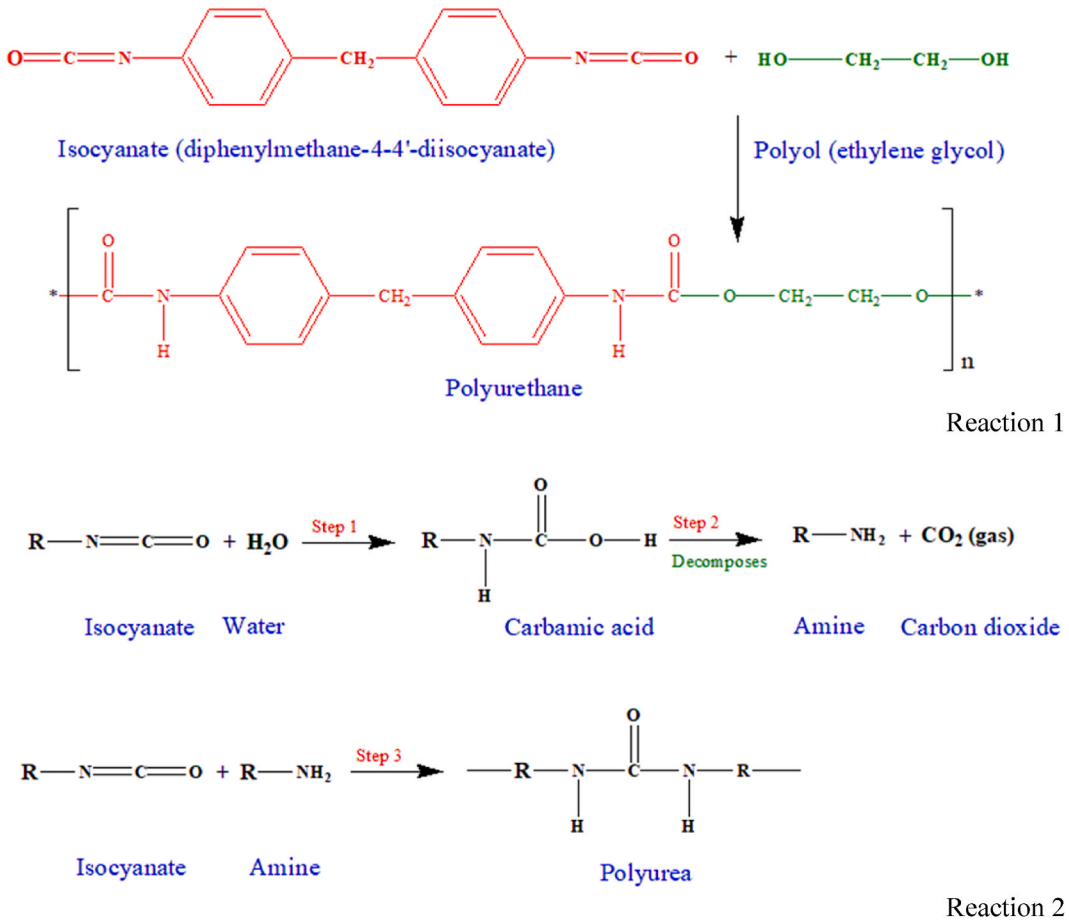

Fig. 5. Polyurethane synthesis reaction mechanism.

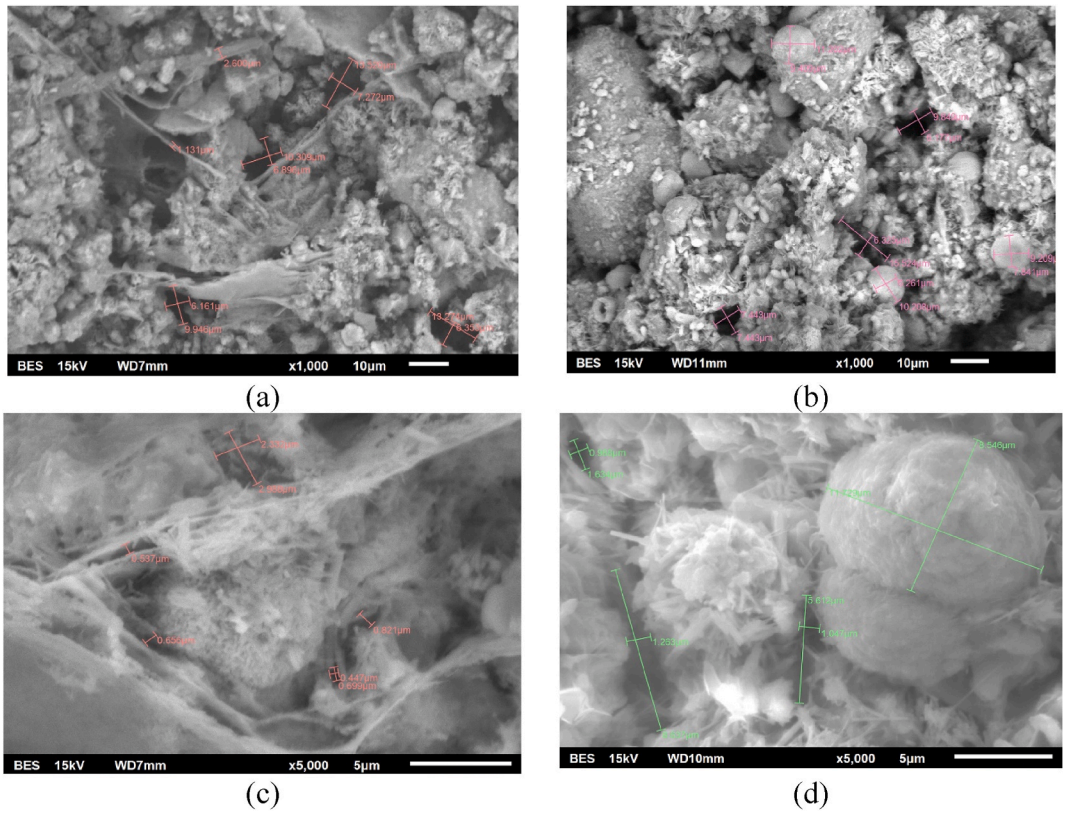

Fig. 6. Micrograph comparison of hybrid foam concrete panels at 1000 magnification; (a) with RHA, (b) without RHA and at 5000 magnification; (c) with RHA (d) without RHA.

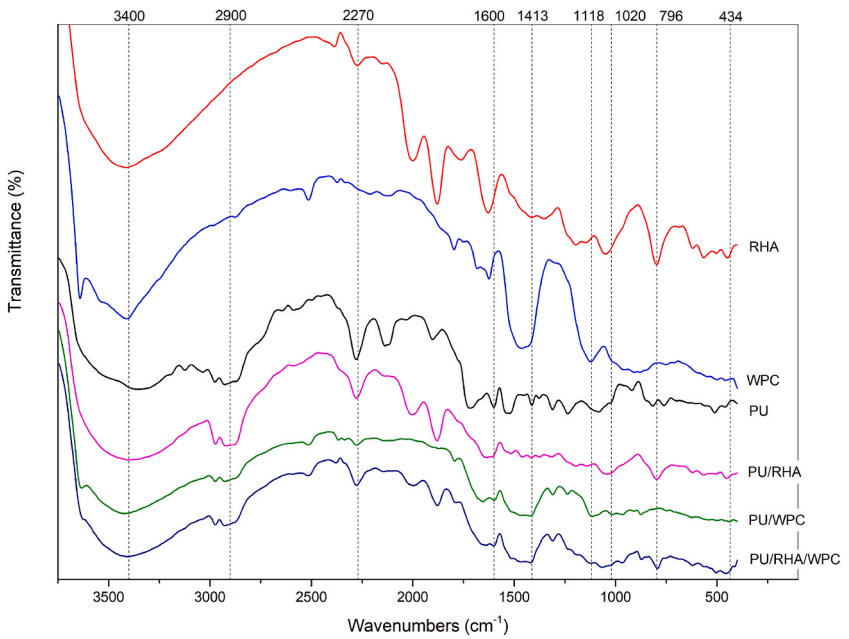

Fig. 7. FT-IR plot of the panel with various concentrations of RHA.

polyurethane although at the same time also occurs other reactions; the cement hydration, carbonation, and pozzolanic activity of the RHA. Physically, the polyurethane bubbles were smaller than within the control (without cement). This might be due to a competition involving water in several reactions and cement causes the bubble smaller. Water was utilized as a blowing agent in polyurethane foam formation and water was also fully involved in the cement hydration reaction. These reactions only occur in a limited condition by involving their essential components. For example, polyurethane polymerization reactions generally involve polyols and isocyanates according to polymerization theory [47], while cementation reactions only occur between C_3S to product C–S–H by hydration of H_2O and carbonating CaO to form $CaCO_3$ as described in the literature [48].

The presence of silica in the sample came from RHA, showing stretching vibration of silica (Si–O) appearing in 434 cm^{-1} and 1020 cm^{-1} [29]. Meanwhile, the Si–*O*–Si for pure RHA revealed 796 cm^{-1} and 870 cm^{-1} for Si–*O*–Si vibration of C–S–H in RHA-WPC [49].

3.3. X-ray diffraction (XRD) analysis

XRD analysis of the HFP uncovered the SiO_2 peaks (20.50° to 21.80°), and the intensity was proportional to RHA content (Fig. 8). The intensity continuously increases up to 20% of the RHA proportion, but the intensity slightly decreased at the ratio of >50% RHA content. The HFP diffractogram recorded several other peaks representing the impurity components since it consistently existed in all samples, including in the 0% RHA sample. HFP crystallinity consistently enhances and SiO_2 diffractogram intensity follows the RHA proportion in the composite. The main components that existed from the precursor (WPC) were Alite (Ca_3O_5Si or Tricalcium silicon pentaoxide/C_3S), $Ca(OH)_2$, and calcite ($CaCO_3$) as shown in Table 2. In the composite, WPC reacted with water which is known as a hydration reaction, and produced majorly C–S–H gel. This reaction has been recognized in many journals [16,50] The evidence of this reaction is shown in XRD diffractogram with intensity from 29.40° to 34.50° and 47.20° and others. Other compounds including Fe_2O_3, MgO, and $CaSO_3$, also showed high intensity in the range of 30° and 35° angles (Fig. 8).

As depicted in Fig. 8, the activity of both primary and secondary hydration reactions has been identified based on the XRD diffractogram. C–S–H and $Ca(OH)_2$ compounds were products of the hydration reaction, and C_3S was the reactant. The cement hydration reaction has the following chemical reaction formula:

$H_2O + C_3S/C_2S \rightarrow Ca(OH)_2 +$ majorly C–S–H gel (hydration reaction). Meanwhile, the secondary hydration reaction in the presence of pozzolanic activity is.

$Ca(OH)_2 + H_2O +$ RHA (SiO_2) → minor C–S–H gel [15].

C–S–H and $Ca(OH)_2$ existed in the HFP diffractogram but C–S–H was dominant as shown at angles of 29.40° and 34.50°.

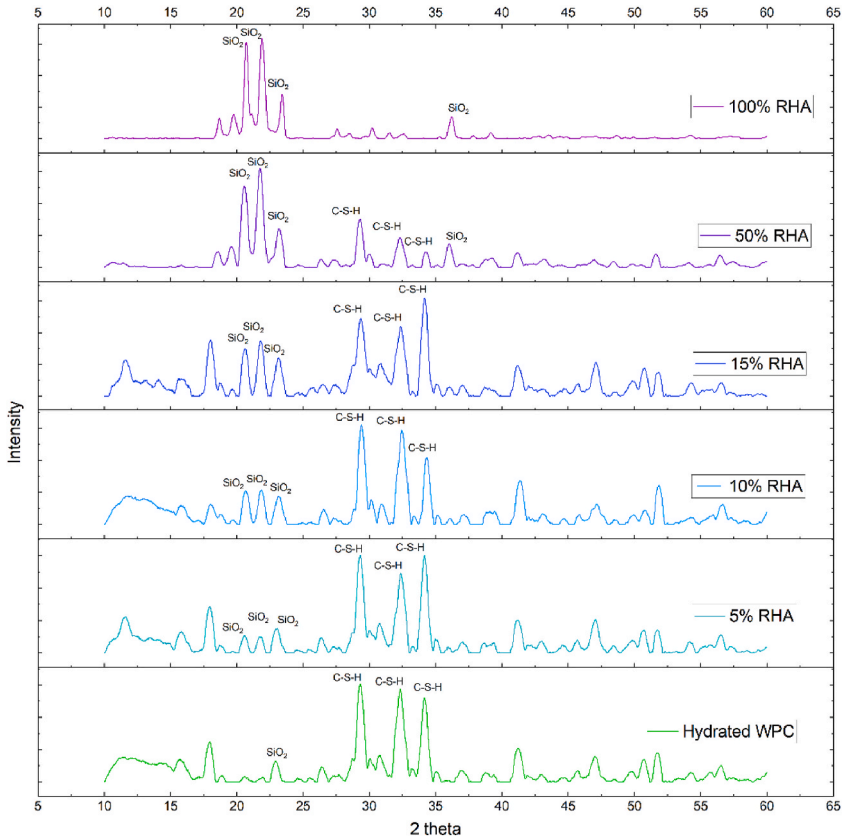

Fig. 8. Diffractogram of the panel with varied the rice husk ash.

3.4. HFP physical and mechanical characteristics

3.4.1. Thermal conductivity

The measurement scheme and specimen of HFP are shown in Fig. 2. The physical and mechanical properties of HFP at various compositions are summarized in Table 3. HFP thermal conductivity was measured to study how much heat was brought by the HFP from the warm wall into the room if HFP will be as a heat block indoors. Table 3 shows that HFP with ≥5% RHA content blocks nearly 50% heat compared with the control according to the thermal conductivity decline. The heat-blocking effect becomes stronger after the 20% RHA ratio in the composition. Also, as presented in Fig. 9, the thermal conductivity of the HFP decreased consistently when the RHA content increased. The reduction was 60.11%, from 0.623 W/mK at 0% RHA to 0.374 W/mK at 5% RHA. Then, it continuously decreased to 0.222 W/mK at 100% of RHA. In this regard, it is reasonable that polyurethane content causes decreased thermal conductivity since polyurethane is organic polymer material and generates foam that reduces surface contact of material from the heat source. Besides, polyurethane and RHA work best together to reduce thermal conductivity. The decrease in thermal conductivity occurs along with the increase in the number of RHA proportions caused by the panel density, which also decreases with increasing RHA. The decrease in density results from the increased number of cavities in the panel. The presence of these voids inhibits heat from reaching other parts of the panel. Then, a comparison of the thermal conductivity of HFP with other composites is explained in Table 4.

According to Table 4, by maintaining the appropriate composition between RHA and polyurethane, HFP had lower thermal conductivity (0.37–0.29 W/mK) than the individual components. The constituent thermal conductivity including concrete only, the polyurethane-Portland cement, and RHA is 0.99 W/mK, 0.62 W/mK, and 1.5–2.75 W/mK respectively as shown in Table 4. This finding is consistent with the previous report that a certain proportion of RHA in concrete could reduce thermal conductivity [18,20,52].

3.4.2. Infra-Red irradiation heat

As discussed in the introduction, HFP is studied to propose as indoor panels to block solar heat penetration from the warm wall into the room. Unlike the thermal conductivity experiment discussed, where the source of heat was an electrical hot plate, in this experiment, the source of heat is IR radiation. Since the sun ray composition is IR dominant but it is not easy to control the intensity, in this section, the radiation was from IR lamps instead of direct sun rays. The effect RHA content of HFP on heat absorption was compared. A plot of the HFP temperature and the irradiation time at each composition of HFP is presented in Fig. 10. The HFP temperature declined along with the enhancement of RHA content.

The expected properties for a sun-heat-blocker in tropical regions is a material that does not absorb sun ray heat or absorbed it but quickly releases it to avoid the room turning warm. Data in Fig. 10 shows that HFP less absorbed heat at higher RHA content and releases it. The temperature of HFP (without RHA) reached up to 55 °C after 200 min after irradiation. Although the lowest temperature of HFP was at 100% RHA content, the medium RHA content (20%) is required to compromise with other HFP physical parameters.

Decreasing heat absorption in the presence of RHA is related to the HFP porosity enhancement as shown in Table 3. Thermal conductivity also represents the HFP to store and release heat [19,20]. The existence of polyurethane, which is low thermal conductivity (0.021–0.032 W/mK) [8], and the presence of voids from foam bubbles within the composite, all contribute to reducing the HFP thermal conductivity.

3.4.3. Thermogravimetric analysis (TGA)

Thermogravimetric analysis for HFP was performed to observe its fire-retardant properties. HFP contains polyurethane with a low melting point (57 °C) and a glass transition temperature of −63 °C [55] was suspected as a flammable material. Then, TGA was recorded and the HFP weight pattern loss at elevated temperatures is presented in Fig. 11. The HFP gravimetric curve for the 100% RHA sample was present in the single-stage decomposition, while HFP with 0%, 20%, and 50% RHA showed the two-stage process.

The first stage occurred in the temperature range of 100 °C–140 °C, indicating the hydration of H_2O compounds from $CaSiO_3.H_2O$ (C–S–H) as the main product of the cementation reaction in the HFP [56]. Then, the second stage took place at the range temperature of 248.72–280.99 °C (for 0%, 20%, and 50% RHA) and at 319.65 °C (100% RHA), in which the data details can be seen in Table 5. The data trend is subject to the polyurethane content at high temperatures [11].

RHA affected slower HFP weight loss while heating at high temperatures and RHA increased the thermal stability of HFP. This finding suggests that the higher proportion of RHA, the better the thermal stability at high temperatures. The presence of RHA silica inhibits the polyurethane from being decomposed easily at high temperatures.

Table 3
The physical and mechanical properties of HFP.

Sample Codes	RHA (%)	Thermal conductivities (W/mK)	Compressive strengths (MPa)	Porosities (%)	Densities (kg/m^3)
HFP 0	0	0.62 ± 0.15	12.37 ± 0.61	10.51 ± 0.57	1351.92 ± 22.68
HFP 5	5	0.37 ± 0.08	11.35 ± 0.22	13.35 ± 0.46	1345.07 ± 22.59
HFP 10	10	0.35 ± 0.06	9.98 ± 0.13	19.43 ± 0.33	1338.18 ± 10.08
HFP 15	15	0.32 ± 0.04	9.42 ± 0.38	21.79 ± 0.16	1279.31 ± 19.03
HFP 20	20	0.32 ± 0.04	7.25 ± 0.25	25.53 ± 0.70	1264.83 ± 5.67
HFP 50	50	0.29 ± 0.03	5.27 ± 0.28	32.80 ± 0.93	1237.11 ± 1.62
HFP 100	100	0.22 ± 0.01	2.40 ± 0.10	61.87 ± 2.59	1216.38 ± 19.00

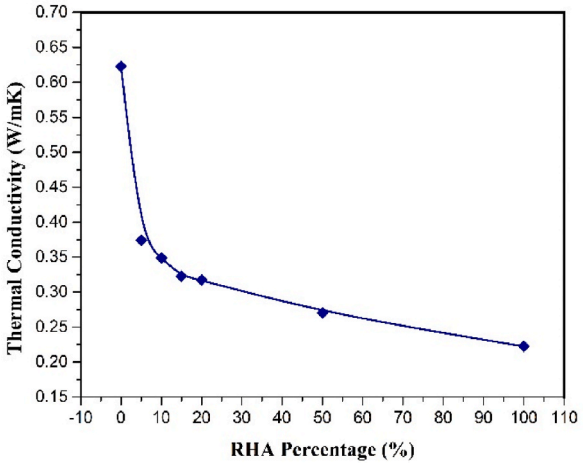

Fig. 9. Effect of RHA percentage on the thermal conductivity.

Table 4
Comparison of thermal conductivity of HFP with other composites.

Composites	Thermal conductivity (W/mK)	References
Polyurethane + 100% WPC, (0% RHA)	0.62	This study
Polyurethane + 100% RHA, (0% WPC)	0.22	This study
Concrete only	0.99	[51]
Foam concrete + RHA (5–15%)	0.19 to 0.17	[52]
Mortar + RHA (10–100% RHA)	0.81–0.17	[20]
White concrete (WPC)	0.75	[31]
RHA only	1.50 to 2.75	[53]
Polyurethane foam only	0.02–0.03	[8]
A mixture of cement, aggregate, and saturated liquid polyurethane	0.60–1.24	[54]

WPC = white Portland cement.

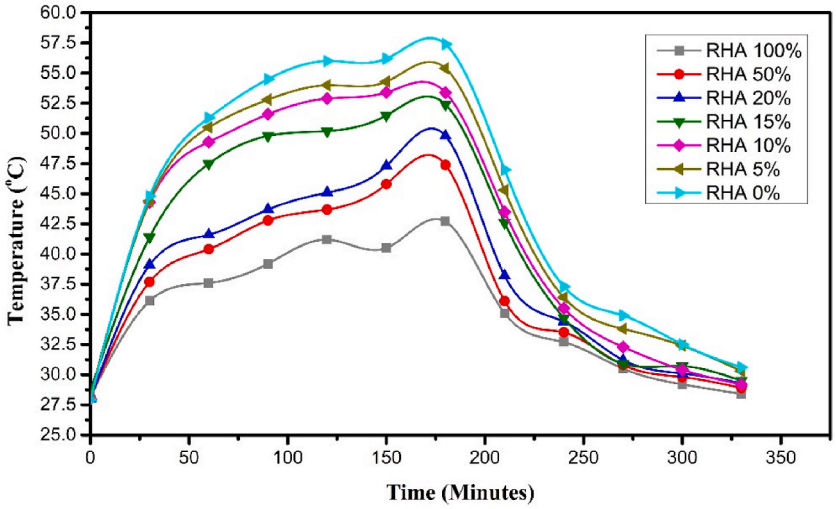

Fig. 10. The Profile of HFP absorbed and desorbed heat from IR radiation.

Fig. 11 also shows that HFP with high content of RHA was not quickly burnt. It stood without significant decomposition up to 300 °C. HFP contained polyurethane and Portland cement, the dehydration started at 100 °C and burned initially at around 300 °C. Therefore, the HFP had relatively fire retardation properties almost at any proportion of RHA. The fire retardation properties were higher than the melting point of polyurethane itself.

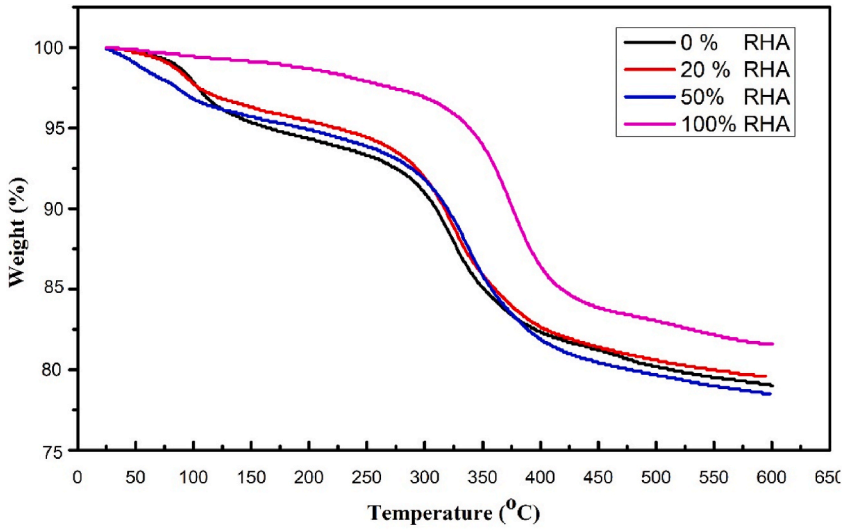

Fig. 11. Thermogravimetric profile of HF panel with various RHA proportion.

Table 5
The onset, endset temperature, and weight loss for each variation in the RHA proportion in the HFP recorded at the TGA instrument.

RHA (%wt)	Onset decomposition temperature (°C)	Endset decomposition temperature (°C)	Weight loss	
			(mg)	(%)
0	248.72	380.21	2.09	20.90
20	259.41	385.41	2.04	20.38
50	280.99	394.56	2.13	21.34
100	319.65	417.52	1.84	18.40

3.4.4. Compressive strength test

Increasing HFP porosity might affect physical strength. Thereby, HFP strength mechanical properties were also measured. The measurements were made only for mixtures with a curing period of 28 days, and the test method refers to the ASTM C-109-02 standard. The shape of the specimen (Fig. 12 (a)) and the test equipment used is portrayed in Fig. 12 (b).

HFP compressive strength data are tabulated in Table 3 and the data trend is presented in Fig. 13. HFP compressive strength decreased gradually, followed by the enhancement of RHA composition. Compressive strength testing aims to measure the strength level of HFP as a requirement for physical properties and perceive compliance with building material standards.

Since the heat blockage materials previously reported are not in uniform dimensions among each other, then their compressive strength and thermal conductivities might not be simply compared with the HFP properties. However, roughly, HFP has relatively

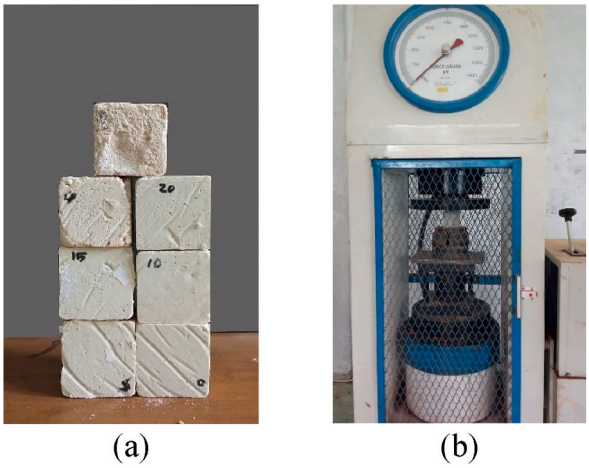

Fig. 12. (a) Prepared Samples and (b) measurement process of compressive strength.

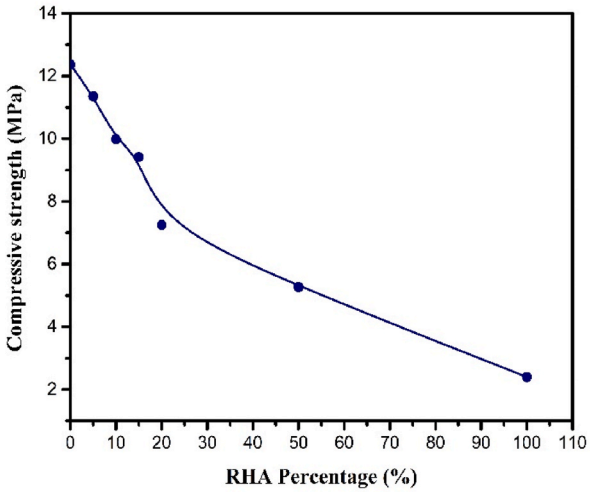

Fig. 13. The plot of compressive strength parameter of HFP with RHA content.

moderate thermal conductivity and higher compressive strength as shown in Table 6.

Since the purpose of this study is to prepare foam lightweight of thermal insulation building materials, the minimum HFP characteristics of concrete strength are referred to the American Concrete Institute (ACI) Committee 213 Guide for Structural Lightweight Aggregate Concrete standard. The density standard is from 300 to 2000 kg/m^3 and the compressive strength standard is 0.7–60 MPa. Hence, the concrete classification based on compressive strength and density can be categorized into three categories, low-density concretes (compressive strength ≈ 0.7–2.0 MPa and density ≈ 300–800 kg/m^3), moderate-strength concretes (compressive strength ≈ 7–14 MPa and density ≈ 800–1350 kg/m^3) and structural concretes (compressive strength ≈ 17–63 MPa and density ≈ 1350–1920 kg/m^3) [59,60].

The compressive strength of the HFP with an RHA proportion of 0–20% met the standard strength for non-structural use, which is in the range of 7.25–12.37 MPa categorizing as moderate strength. The HFP with RHA content of 20%–100% showed low density referring to its compressive strength of 2.40–7.00 MPa, as verified in the previous study [20].

3.5. Density and porosity

Two contradicting parameters, i.e., the density and porosity of the composite, were considered in this study. Density determination was carried out using the ASTM C567-05a (2005) standards, and for the porosity, ASTM C 642–06 (2008) standard was used. Porosity is influenced by the number of cavities formed in the panel. The porosity determination was then carried out by calculating the amount of water absorption by the cavities in the panel—the more holes, the greater the possibility of being filled in with air. The void existence decreases the thermal conductivity of the panels [20].

HFP Density and porosity data, which are two interconnected parameters are displayed in Table 3. High porosity is usually followed by low density and reversely. High porosity is also preferable for heat insulator properties, but high density contributes to physical strength. Moreover, density and porosity strongly influence the strength and thermal conductivity of RHA-based HFP. The lower the density of a material, the higher the porosity, as shown in Fig. 14 (a) and **(b)**. This finding has been confirmed by the research previously [34].

Here, the presence of RHA significantly affected the porosity and density of the HF panel. Also, the RHA content, particle size, and surface area all affect water absorption. The smaller the particle size, and the higher the content of RHA (>20%), the more water absorb [61], and the higher HFP porosity.

Table 6
Comparison of mechanical properties of HFP with various concrete foams.

Composite formula	Thermal conductivity (W/mK)	Compressive strength (MPa)	Ref
Material included-glass fiber-reinforced foam concrete, with dimensions of (50 × 50 × 50 mm)	0.153	2.52	[57]
Foam Concrete Produced with Recycled Concrete Powder and Phase Change Materials; dimension (40 × 40 × 160 mm)	0.242–0.347	1.41–6.95	[5]
Foam concretes containing expanded vermiculite powder and silica fume; dimension (200 × 200 × 500 mm prism and cylinder with Ø150 300 mm)	0.05–0.24	0.5–4.0	[58]
Hybrid foam panel made of polyurethane-hybrid-foam-concrete and rice-husk-ash; dimension for thermal conductivity (diameter = 60 cm; thickness = 5 cm), dimension for compressive strength (50 × 50 × 50 mm)	0.22–0.62	2.5–12.5	This study

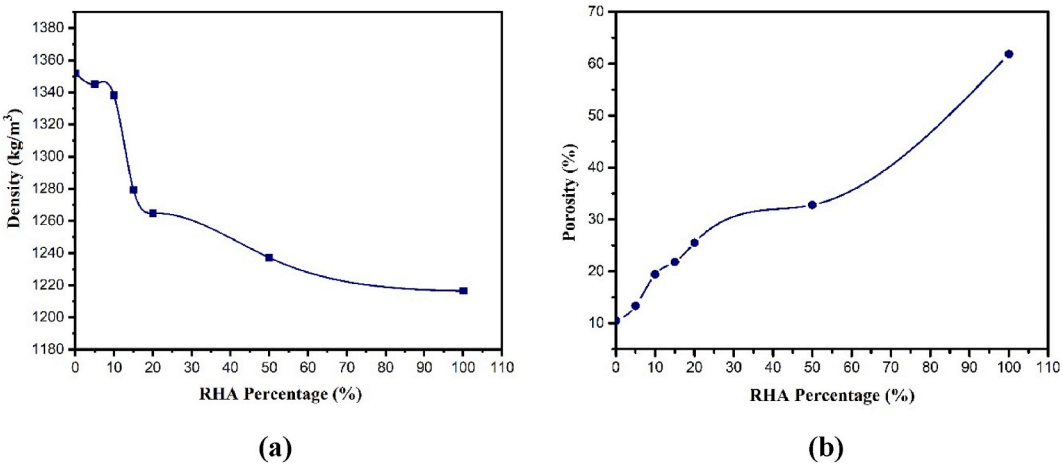

Fig. 14. (a) HFP density and (b) porosity.

4. Conclusion

Synthesis of thermal insulation panels with RHA, polyurethane, and white cement as the base material has been successfully fabricated and shows interesting characteristics. Since the key for HFP pore formation is the chemical reactions of the component, then the formation of polyurethane from a reaction between polyol and isocyanate confirmed occurred along with the hydration/carbonation reaction of cement and the secondary hydration reaction of RHA pozzolanic activity. HFP absorbed heat slower at the high content of RHA and released heat faster at low RHA content. HFP containing 20 wt% of RHA blocked IR radiation heat significantly and moderately released it, also it has acceptable compressive strength. With this RHA composition, the HFP compressive strength met the standards for non-structural uses, such as thermal insulation materials. Also, the HFP stands for heat at least 300 °C without excessively burning. HFP is potentially used for indoor wall insulation, especially in tropical regions.

Author contribution statement

Jofrishal Jofrishal: Performed the experiments; Wrote the paper.
Muhammad Adlim: Conceived and designed the experiments; Wrote the paper.
Elin Yusibani, Akhyar Akhyar: Analyzed and interpreted the data.
Ratu Fazlia Inda Rahmayani, Rahmatul Fajri: Contributed reagents, materials, analysis tools or data.

Data availability statement

Data included in article/supp. material/referenced in article.

Declaration of competing interest

The authors declare that they have no known competing financial interests or personal relationships that could have appeared to influence the work reported in this paper.

Acknowledgments

The authors express appreciation to the Ministry of Indonesia Education, Culture, Research, and Technology for the scholarship support, to the National Research and Innovation Agency for facilities, scientific and technical support, and to Universitas Syiah Kuala for research fund with grant number 166/UN11/SPK/PNBP/2021, Februari 19, 2021 and 141/UN11/SPK/PNBP/2022, February 11, 2022.

References

[1] K. Lee, Y. Kim, H.C. Sung, R. Jang, J. Ryu, S.W. Jeon, Trend analysis of urban heat island intensity according to urban area change in Asian mega cities, in: 40th Asian Conf. Remote Sensing, ACRS 2019 Prog. Remote Sens. Technol. Smart Futur., Vol. 12, no. 1, 2020, pp. 1–11.
[2] Y. Qin, Y. Zhao, X. Chen, L. Wang, F. Li, T. Bao, Moist curing increases the solar reflectance of concrete, Construct. Build. Mater. 215 (2019) 114–118, https://doi.org/10.1016/j.conbuildmat.2019.04.164.
[3] US EPA, Heat Island Cooling Strategies, United States Environmental Protection Agency, 2019. https://www.epa.gov/heat-islands/heat-island-cooling-strategies. (Accessed 7 January 2020).

[4] H. Yousefian, D. Rodrigue, Hybrid composite foams based on nanoclays and natural fibres, Eng. Mater. (2016) 51–79, https://doi.org/10.1007/978-981-10-0950-1_3.
[5] O. Gencel, et al., Foam concrete produced with recycled concrete powder and phase change materials, Sustain. Times 14 (12) (2022), https://doi.org/10.3390/su14127458.
[6] H. Yang, Z. Hu, S. Chen-cheng, H. Sheng-bo, Y. Jing-xing, Pore structure of nano-porous thermal insulating materials and thermal transport via gas phase in their pores, Chinese J. Eng. 61 (6) (2019) 788–796, https://doi.org/10.13374/j.issn2095-9389.2019.06.011.
[7] I.K. Harith, Study on polyurethane foamed concrete for use in structural applications, Case Stud. Constr. Mater. 8 (1) (2018) 79–86, https://doi.org/10.1016/j.cscm.2017.11.005.
[8] H. Zhang, W.Z. Fang, Y.M. Li, W.Q. Tao, Experimental study of the thermal conductivity of polyurethane foams, Appl. Therm. Eng. 115 (2017) 528–538, https://doi.org/10.1016/j.applthermaleng.2016.12.057.
[9] O. Coppola, G. Magliulo, E. Di Maio, Mechanical characterization of a polyurethane-cement hybrid foam in compression, tension, and shear, J. Mater. Civ. Eng. 29 (2) (2017) 1–8, https://doi.org/10.1061/(ASCE)MT.1943-5533.0001738.
[10] F.D.L. Bossa, et al., Greener nanocomposite polyurethane foam based on sustainable polyol and natural fillers: investigation of chemico-physical and mechanical properties, Materials 13 (no. 1) (2020), https://doi.org/10.3390/ma13010211.
[11] M. Verdolotti, Lavorgna, E. Di Maio, S. Iannace, Hydration-induced reinforcement of rigid polyurethaneecement foams: the effect of the co-continuous morphology on the thermal-oxidative stability, Polym. Degrad. Stabil. 98 (1) (2013) 64–72, https://doi.org/10.1016/j.polymdegradstab.2012.10.027.
[12] L. Verdolotti, M.R. Di Caprio, M. Lavorgna, G.G. Buonocore, Polyurethane Nanocomposite Foams: Correlation between Nanofillers, Porous Morphology, and Structural and Functional Properties, Elsevier Inc., 2017, https://doi.org/10.1016/B978-0-12-804065-2.00009-7.
[13] S. Manubothula, M. Gorre, Influence of rice husk ash on compressive strength of an aerated concrete, in: International Conference on Advances in Construction Materials and Structures, 2022, pp. 1982–1986, https://doi.org/10.1016/j.matpr.2022.05.320 [Online]. Available:.
[14] B. Iftikhar, et al., Predictive modeling of compressive strength of sustainable rice husk ash concrete: ensemble learner optimization and comparison, J. Clean. Prod. 348 (2022), 131285, https://doi.org/10.1016/j.jclepro.2022.131285 [Online]. Available:.
[15] M. Amran, et al., Rice husk ash-based concrete composites: a critical review of their properties and applications, Crystals 11 (2) (2021) 1–33, https://doi.org/10.3390/cryst11020168.
[16] S.H. Kang, S.G. Hong, J. Moon, The use of rice husk ash as reactive filler in ultra-high performance concrete, March, Cement Concr. Res. 115 (2019) 389–400, https://doi.org/10.1016/j.cemconres.2018.09.004.
[17] S.A. Zareei, F. Ameri, F. Dorostkar, M. Ahmadi, Rice husk ash as a partial replacement of cement in high strength concrete containing micro silica: evaluating durability and mechanical properties, Case Stud. Constr. Mater. 7 (2017) 73–81, https://doi.org/10.1016/j.cscm.2017.05.001.
[18] K. Selvaranjan, J.C.P.H. Gamage, G.I.P. De Silva, V. Attanayaka, Thermal performance of Rice Husk Ash mixed mortar in concrete and masonry buildings, Bud. i Archit. 19 (4) (2020) 43–52, https://doi.org/10.35784/bud-arch.2121.
[19] G. H. M. J. D. S. Silva, S. Vishvalingam, T. Etampawala, Effect of waste rice husk ash from rice husk fuelled brick kilns on strength, durability and thermal performances of mortar, Construct. Build. Mater. 268 (2021), 121794, https://doi.org/10.1016/j.conbuildmat.2020.121794.
[20] K. Selvaranjan, et al., Thermal and environmental impact analysis of rice husk ash-based mortar as insulating wall plaster, Construct. Build. Mater. 283 (2021), 122744, https://doi.org/10.1016/j.conbuildmat.2021.122744.
[21] G. H. M. J. D. S. Silva, B.V.A. Perera, Effect of waste rice husk ash (RHA) on structural, thermal and acoustic properties of fired clay bricks, J. Build. Eng. 18 (2018) 252–259, https://doi.org/10.1016/j.jobe.2018.03.019. September 2017.
[22] G. H. M. J. D. S. Silva, M.L.C. Surangi, Effect of waste rice husk ash on structural, thermal and run-off properties of clay roof tiles, Construct. Build. Mater. 154 (2017) 251–257, https://doi.org/10.1016/j.conbuildmat.2017.07.169.
[23] A. Raheem, K.O. Oriola, M.A. Kareem, R. Abdulwahab, Investigation on thermal properties of rice husk ash-blended palm kernel shell concrete, Environ. Challenges 5 (2021), 100284.
[24] E.P. Ayswarya, A.B. Nair, E.T. Thachil, A comparative study of mechanical, dynamic mechanical and thermal properties of rice husk ash, modified rice husk ash and nano silica filled epoxy composites, Mater. Today Proc. 47 (2021) 5351–5357, https://doi.org/10.1016/j.matpr.2021.06.067.
[25] K. Yu, Y. Liu, Y. Yang, Enhanced thermal properties of polyethylene glycol/modified rice husk ash eco-friendly form-stable phase change material via optimizing support pore structure, J. Energy Storage 43 (2021), 103172.
[26] M. Szycher, Handbook of Polyurethanes, second ed., Taylor & Francis Group, 2013.
[27] P.A. Adesina, F.A. Olutoge, Structural properties of sustainable concrete developed using rice husk ash and hydrated lime, February, J. Build. Eng. 25 (2019), 100804, https://doi.org/10.1016/j.jobe.2019.100804.
[28] F. Aslam, et al., Compressive strength prediction of rice husk ash using multiphysics genetic expression programming, Ain Shams Eng. J. 13 (3) (2022), 101593, https://doi.org/10.1016/j.asej.2021.09.020.
[29] S.K. Das, et al., Characterization and utilization of rice husk ash (RHA) in fly ash - blast furnace slag based geopolymer concrete for sustainable future, 2nd International Conference on Processing and Characterization of Materials 33 (8) (2020) 5162–5167, https://doi.org/10.1016/j.matpr.2020.02.870.
[30] K. Moresová, F. Škvára, White cement - properties, manufacture, prospects, Ceram. - Silikaty 45 (4) (2001) 158–163.
[31] S. Ibn-Elhaj, S. Mounir, A. Khabbazi, Measurement of thermal conductivity of reed and white cement, The 6th International Congress on Thermal Sciences 2345 (2021) 1–6, https://doi.org/10.1063/5.0049444, 20031.
[32] F. Shaker, A. Rashad, M. Allam, Properties of concrete incorporating locally produced Portland limestone cement, Ain Shams Eng. J. 9 (4) (2018) 2301–2309, https://doi.org/10.1016/j.asej.2017.04.005.
[33] R.P. Jaya, M.A.A. Muhamad Nor, Z.A. Ahmad, Z. Mohd Amin, Properties of mortar containing rice husk ash at different temperature and exposed to aggressive environment, Adv. Mater. Res. 620 (2013) 87–93. January, https://doi.org/10.4028/www.scientific.net/AMR.620.87.
[34] H. Liu, G. Luo, H. Wei, H. Yu, Strength, permeability, and freeze-thaw durability of pervious concrete with different aggregate sizes, porosities, andwater-binder ratios, Appl. Sci. 8 (8) (2018), https://doi.org/10.3390/app8081217.
[35] R.S. Lin, X.Y. Wang, H.S. Lee, H.K. Cho, Hydration and microstructure of cement pastes with calcined Hwangtoh Clay, Materials 12 (3) (2019) 1–19, https://doi.org/10.3390/ma12030458.
[36] A.A. Raheem, K.O. Oriola, M.A. Kareem, R. Abdulwahab, Investigation on thermal properties of rice husk ash-blended palm kernel shell concrete, July, Environ. Challenges 5 (2021), 100284, https://doi.org/10.1016/j.envc.2021.100284.
[37] A. Adesina, Use of Rice Husk in Concrete: Review of Mechanical Properties, 2018. September.
[38] Z.F. Jawad, A.J. Salman, R.J. Ghayyib, M.N. Hawas, Investigation the effect of different nano materials on the compressive strength of cement mortar, March, AIP Conf. Proc. 2213 (2020), https://doi.org/10.1063/5.0000164.
[39] M.M. López, Y. Pineda, O. Gutiérrez, Evaluation of durability and mechanical properties of the cement mortar added with slag blast furnace, Procedia Mater. Sci. 9 (2015) 367–376, https://doi.org/10.1016/j.mspro.2015.05.006.
[40] C.J. Obando, K.E. Kaloush, Estimating the thermal conductivity of asphalt binders, J. Test. Eval. 50 (2) (2022), https://doi.org/10.1520/JTE20210208.
[41] A.Y. Atta, B.Y. Jibril, B.O. Aderemi, S.S. Adefila, Preparation of analcime from local kaolin and rice husk ash, Appl. Clay Sci. 61 (2012) 8–13, https://doi.org/10.1016/j.clay.2012.02.018.
[42] S.S. Hossain, L. Mathur, P.K. Roy, Rice husk/rice husk ash as an alternative source of silica in ceramics: a review, J. Asian Ceram. Soc. 6 (4) (2016) 299–313, https://doi.org/10.1080/21870764.2018.1539210.
[43] R. Muthuraj, C. Lacoste, P. Lacroix, A. Bergeret, Sustainable thermal insulation biocomposites from rice husk, wheat husk, wood fibers and textile waste fibers: elaboration and performances evaluation, Ind. 135 (2019) 238–245, https://doi.org/10.1016/j.indcrop.2019.04.053.
[44] W. Pongdong, C. Kummerlöwe, N. Vennemann, A. Thitithammawong, C. Nakason, Property correlations for dynamically cured rice husk ash filled epoxidized natural rubber/thermoplastic polyurethane blends: influences of RHA loading, Polym. Test. 53 (2016) 245–256, https://doi.org/10.1016/j.polymertesting.2016.05.026.

[45] W. Pongdong, C. Kummerlöwe, N. Vennemann, A. Thitithammawong, C. Nakason, A comparative investigation of rice husk ash and siliceous earth as reinforcing fillers in dynamically cured blends of epoxidized natural rubber (ENR) and thermoplastic polyurethane (TPU), J. Polym. Environ. 26 (3) (2017) 1145–1159, https://doi.org/10.1007/s10924-017-1022-5.
[46] S. Saral, M.P. Indumathi, G.R. Rajarajeswari, Mahua oil-based polyurethane/chitosan/nano ZnO composite films for biodegradable food packaging applications, Int. J. Biol. Macromol. 124 (2019) 163–174, https://doi.org/10.1016/j.ijbiomac.2018.11.195.
[47] R. Rao, et al., The kinetics of polyurethane structural foam formation: foaming and polymerization, Am. Inst. Chem. Eng. J. 63 (7) (2017) 2945–2957, https://doi.org/10.1002/aic.
[48] S. Kashef-Haghighi, Y. Shao, S. Ghoshal, Mathematical modeling of CO2 uptake by concrete during accelerated carbonation curing, January 2015, Cement Concr. Res. 67 (2015) 1–10, https://doi.org/10.1016/j.cemconres.2014.07.020.
[49] K. Khan, et al., Effective use of micro-silica extracted from rice husk ash for the production of high-performance and sustainable cement mortar, Construct. Build. Mater. 258 (2020), 119589, https://doi.org/10.1016/j.conbuildmat.2020.119589.
[50] A.S. Gill, R. Siddique, Durability properties of self-compacting concrete incorporating metakaolin and rice husk ash, Construct. Build. Mater. 176 (2018) 323–332, https://doi.org/10.1016/j.conbuildmat.2018.05.054.
[51] S. Lanjekar, S. Kadam, Effect of polyurethane foam addition on thermal conductivity of concrete, Int. J. Res. Sci. Innov. 5 (7) (2018) 38–41.
[52] N.R. Aravind, D. Sathyan, K.M. Mini, Rice husk incorporated foam concrete wall panels as a thermal insulating material in buildings, Indoor Built Environ. 29 (5) (2020) 721–729, https://doi.org/10.1177/1420326X19862017.
[53] M.R.F. Gonçalves, C.P. Bergmann, Thermal insulators made with rice husk ashes: production and correlation between properties and microstructure, Construct. Build. Mater. 21 (12) (2007) 2059–2065, https://doi.org/10.1016/j.conbuildmat.2006.05.057.
[54] P. Mounanga, W. Gbongbon, P. Poullain, P. Turcry, Proportioning and characterization of lightweight concrete mixtures made with rigid polyurethane foam wastes, Cem. Concr. Compos. 30 (9) (2008) 806–814, https://doi.org/10.1016/j.cemconcomp.2008.06.007.
[55] Polymer properties database, "Polyurethane," polymerdatabase.com. 2022. https://polymerdatabase.com/polymer classes/Polyurethane type.html (Accessed 29 March 2022).
[56] L. Verdolotti, E. Di Maio, G. Forte, M. Lavorgna, S. Iannace, Hydration-induced reinforcement of polyurethane-cement foams: solvent resistance and mechanical properties, J. Mater. Sci. 45 (12) (2010) 3388–3391, https://doi.org/10.1007/s10853-010-4416-5.
[57] O. Gencel, et al., Development, characterization and thermo-regulative performance of microencapsulated phase change material included-glass fiber reinforced foam concrete as novel thermal energy effective-building material, Energy 257 (2022), 124786, https://doi.org/10.1016/j.energy.2022.124786.
[58] F. Koksal, Y. Sahin, O. Gence, Influence of expanded vermiculite powder and silica fume on properties of foam concretes, Construct. Build. Mater. 257 (2020), 119547, https://doi.org/10.1016/j.conbuildmat.2020.119547.
[59] A. Chaipanich, P. Chindaprasirt, The Properties and Durability of Autoclaved Aerated Concrete Masonry Blocks, Elsevier Ltd, 2015, https://doi.org/10.1016/B978-1-78242-305-8.00009-7.
[60] N.R. Iyer, An Overview of Cementitious Construction Materials, INC, 2020, https://doi.org/10.1016/B978-0-12-818961-0.00001-6.
[61] A. Balraj, D. Jayaraman, J. Krishnan, J. Alex, Experimental investigation on water absorption capacity of RHA-added cement concrete, Environ. Sci. Pollut. Res. 28 (45) (2021) 63623–63628, https://doi.org/10.1007/s11356-020-11339-1.